
This is an electronic reprint of the original article.
This reprint may differ from the original in pagination and typographic detail.

Luotonen, Otso I.V.; Greca, Luiz G.; Nyström, Gustav; Guo, Junling; Richardson, Joseph J.; Rojas, Orlando J.; Tardy, Blaise L.

Benchmarking supramolecular adhesive behavior of nanocelluloses, cellulose derivatives and proteins

Published in:
Carbohydrate Polymers

DOI:
[10.1016/j.carbpol.2022.119681](https://doi.org/10.1016/j.carbpol.2022.119681)

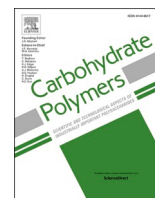
Published: 15/09/2022

Document Version
Publisher's PDF, also known as Version of record

Published under the following license:
CC BY

Please cite the original version:
Luotonen, O. I. V., Greca, L. G., Nyström, G., Guo, J., Richardson, J. J., Rojas, O. J., & Tardy, B. L. (2022). Benchmarking supramolecular adhesive behavior of nanocelluloses, cellulose derivatives and proteins. *Carbohydrate Polymers*, 292, 1-9. Article 119681. <https://doi.org/10.1016/j.carbpol.2022.119681>

This material is protected by copyright and other intellectual property rights, and duplication or sale of all or part of any of the repository collections is not permitted, except that material may be duplicated by you for your research use or educational purposes in electronic or print form. You must obtain permission for any other use. Electronic or print copies may not be offered, whether for sale or otherwise to anyone who is not an authorised user.



Benchmarking supramolecular adhesive behavior of nanocelluloses, cellulose derivatives and proteins

Otso I.V. Luotonen^a, Luiz G. Greca^a, Gustav Nyström^{b,c}, Junling Guo^d, Joseph J. Richardson^e, Orlando J. Rojas^{a,f,*}, Blaise L. Tardy^{a,g,h,*}

^a Department of Bioproducts and Biosystems, School of Chemical Engineering, Aalto University, P. O. Box 16300, FI-00076 Aalto, Finland

^b Laboratory for Cellulose & Wood Materials, Empa – Swiss Federal Laboratories for Materials Science and Technology, Überlandstrasse 129, 8600 Dübendorf, Switzerland

^c Department of Health Science and Technology, ETH Zürich, 8092 Zürich, Switzerland

^d BMI Center for Biomass Materials and Nanointerfaces, College of Biomass Science and Engineering, Sichuan University, Chengdu 610065, China

^e Department of Materials Engineering, School of Engineering, University of Tokyo, Tokyo 113-8656, Japan

^f Bioproducts Institute, Department of Chemical and Biological Engineering, Department of Chemistry and Department of Wood Science, University of British Columbia, 2360 East Mall, Vancouver, BC V6T 1Z4, Canada

^g Khalifa University, Department of Chemical Engineering, Abu Dhabi, United Arab Emirates

^h Research and Innovation Center on CO₂ and Hydrogen, Khalifa University, Abu Dhabi, United Arab Emirates

ARTICLE INFO

Keywords:

Natural polymers
Biopolymers
Cellulose
Carbohydrate
Nanocellulose
Nanocrystal
Cellulose derivatives

ABSTRACT

One of the key steps towards a broader implementation of renewable materials is the development of biodegradable adhesives that can be attained at scale and utilized safely. Recently, cellulose nanocrystals (CNCs) were demonstrated to have remarkable adhesive properties. Herein, we study three classes of naturally synthesized biopolymers as adhesives, namely nanocelluloses (CNFs), cellulose derivatives, and proteins by themselves and when used as additives with CNCs. Among the samples evaluated, the adhesion strength was the highest for bovine serum albumin and hydroxypropyl cellulose (beyond 10 MPa). These were followed by carboxymethylcellulose and CNCs (ca. 5 MPa) and mechanically fibrillated CNFs (ca. 2 MPa), and finally by tempo-oxidized CNFs (0.2 MPa) and lysozyme (1.5 MPa). Remarkably, we find that the anisotropy of adhesion (in plane vs out of plane) falls within a narrow range across the bio-based adhesives studied. Collectively, this study benchmarks bio-based non-covalent adhesives aiming towards their improvement and implementation.

1. Introduction

As the global economy transitions towards sustainable materials, natural biopolymers resulting from natural biosynthetic processes are gaining increased attention due to their renewable nature and inherent biodegradability (Tardy et al., 2021). The need to replace synthetic materials is imminent, as hazardous plastics are currently mass-produced despite their short service-life and uncontrolled end-of-life, which collectively lead to the introduction of contaminants into ecosystems and food chains (Cole, Lindeque, Halsband, & Galloway, 2011; Geyer, Jambeck, & Law, 2017). The dramatic increase in plastic use for short service-life items in packaging and logistics in the post-COVID era (valued at over \$59 billion USD in 2020) highlights the urgent need to better understand and utilize natural biopolymers. In particular, the

interfacial non-covalent interactions of bio-colloids and natural biopolymers are what dictate their ability to form high strength bonds with themselves (cohesive) and at other interfaces (adhesive) (Daicho, Kobayashi, Fujisawa, & Saito, 2021; Greca et al., 2021; Mittal et al., 2018; Tardy et al., 2020). High overall strength can be achieved by an array of noncovalent bonds which are individually relatively weak (Wang et al., 2019), and different bio-colloids and biopolymers can be consolidated through confined evaporative processes into structures of multi-scale order. Across different applications, such non-covalent, supramolecular, interactions determine the performance of natural fibre based composites (Mattos et al., 2020; Siqueira et al., 2017; Yang et al., 2021), natural polymers assemblies (Beaumont et al., 2021; Chen et al., 2020; Korhonen, Sawada, & Budtova, 2019), and the formation of natural adhesives and binders (Greca et al., 2021; Tardy et al., 2020).

* Corresponding authors at: Department of Bioproducts and Biosystems, School of Chemical Engineering, Aalto University, P. O. Box 16300, FI-00076 Aalto, Finland.

E-mail addresses: orlando.rojas@ubc.ca (O.J. Rojas), blaise.tardy@ku.ac.ae (B.L. Tardy).

<https://doi.org/10.1016/j.carbpol.2022.119681>

Received 14 March 2022; Received in revised form 14 May 2022; Accepted 28 May 2022

Available online 1 June 2022

0144-8617/© 2022 The Authors. Published by Elsevier Ltd. This is an open access article under the CC BY license (<http://creativecommons.org/licenses/by/4.0/>).

Recently, the self-assembly of bio-colloids such as nanocellulose has been explored to form adhesives between glass, and other hydrophilic surfaces, upon directionally controlled drying of the dispersion, i.e. using confined evaporation-induced self-assembly (C-EISA, Beisl, Adamczyk, Friedl, & Ejima, 2020; Tardy et al., 2020). Although the adhesives exploit non-covalent interactions, the shear strength can reach up to 9 MPa. Natural biopolymers, such as proteins, carbohydrate polymers, and their biocolloidal supramolecular assemblies are largely biosynthesized building blocks that are also industrially produced in large quantities (Ajdari, Tardy, Mattos, Bai, & Rojas, 2021; Li et al., 2021; Tardy et al., 2021). Most of these biomacromolecular constructs are water soluble/dispersible, which allows for aqueous processing into different materials based on the interfacial interactions and rheology of the bio-colloidal building block suspensions (Gençer, Schütz, & Thielemans, 2017; Greca et al., 2021; Klockars et al., 2019; Tardy et al., 2017, 2020). While their assembly and associated materials properties have been intensely studied over the past decade, there are no benchmarks for the performance of their interfacial interactions. This knowledge gap in interfacial interactions is untimely due to the rising demand for bio-based adhesives to provide green solutions for bonding systems in various industries.

Herein, we aimed to address this gap by evaluating the adhesive properties of a range of distinctly different classes of bio-colloids and biomacromolecules (Fig. 1a). We also explore their impact as additives in combination with CNC, with the goal of highlighting potential synergies. This is expected to provide insights into the overarching design principles underpinning bio-colloidal adhesives, including e.g. considerations on the effect of disordered aggregation induced by the presence of the additive prior to assembly and during joint formation. We specifically evaluated on their own or as composites with CNCs: (1) higher aspect-ratio nanocellulose, such as mechanically fibrillated cellulose nanofibres (CNFs) with four degrees of fibrillation, which were previously shown to also impart higher toughness when added into CNC materials (Mattos et al., 2020; Natarajan et al., 2018), (2) two well established model proteins, namely bovine serum albumin (BSA, isoelectric point (IP) 4.7 (Yasun et al., 2015), MW 66 kDa) and lysozyme (IP 11.7 (Felsovalyi, Mangiagalli, Bureau, Kumar, & Banta, 2011), MW 14.4

kDa), and (3) cellulose derivatives, namely carboxymethylcellulose (CMC (Cheng, Wyckoff, Dowd, & He, 2019; Filpponen et al., 2012; Mittal & Pizzi, 2003)) and hydroxypropyl cellulose (HPC (Dore, Dörling, Garcia-Pomar, Campoy-Quiles, & Mihi, 2020; Espinha et al., 2018; Walters, Boott, Nguyen, Hamad, & MacLachlan, 2020; Yi et al., 2019)). Proteins see much attention as potential sources of novel adhesives, and more specifically BSA can produce strong adhesion on its own (Roberts et al., 2020), while lysozyme has been studied together with cellulose and chitin nanocrystals to produce films and adhesives (De France, Kummer, Ren, Campioni, & Nyström, 2020; Greca et al., 2021). The aim of using cellulose derivative was to provide a softer matrix potentially improved the toughness of CNC-only joints. These natural biopolymers are typically available at low costs at commercial scales and cover a distinct gelation concentration range, corresponding to lower than 1% for TOCNF to above 50% for BSA, making them suitable benchmarks for future studies.

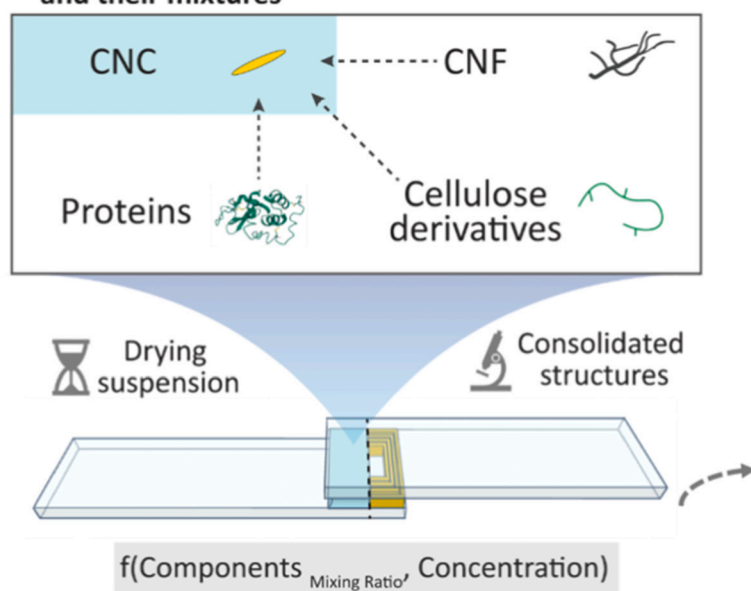
The joints were evaluated for their long-range order, contact area, lap-shear strength, and out-of-plane adhesive strength. Meta-analysis of the adhesive strength was performed by normalizing the load to the actual load-bearing or contact areas, which enabled us to provide clear guidelines on what are the key features to look for in natural biopolymers for the design of high strength adhesive formulations. Importantly, the anisotropy of adhesion of evaluated systems, i.e. their out-of-plane strength vs shear-strength (Fig. 1b) was analysed to illustrate the principles governing supramolecular interaction of natural biopolymers, which may bear similarities regardless of their conformation, size, or other physicochemical properties (Fig. 1b).

2. Experimental

2.1. Materials

CNCs (ca. 10%, w/v) were acquired through the Process Development Center, University of Maine, USA (FPL, Madison, WI). These have been characterized in a previous study: length and width 134 ± 52 nm and 7 ± 2 nm resp., sulfate half-ester content 335 mmol/kg, zeta potential ca. -47 mV (Reid, Villalobos, & Cranston, 2017). Mechanically

a) C-EISA of bio-colloids, bio-macromolecules and their mixtures



b) Supramolecular anisotropic adhesion

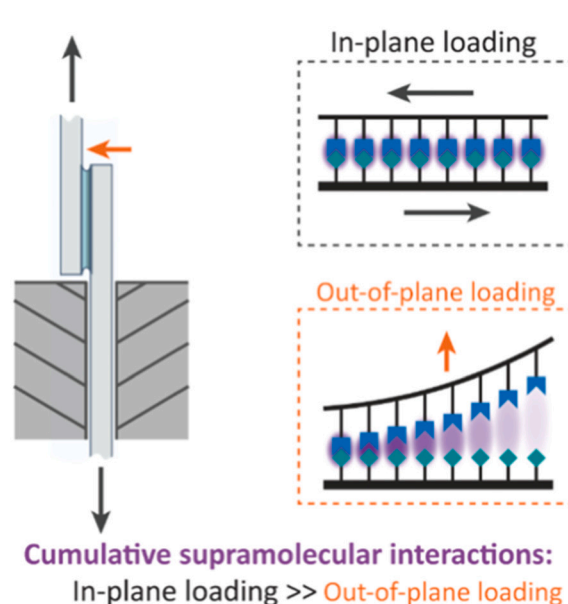


Fig. 1. (a) Adhesion of glass surfaces using various bio-colloids and bio-macromolecules with C-EISA (confined evaporation-induced self-assembly). (b) Their adhesion strength was measured under in-plane and out-of-plane loads highlighting distinct mechanisms of failure, which can be ascribed to the dynamic interfacial interactions of the biomacromolecules.

fibrillated CNFs were prepared by mechanical disintegration from never-dried, fully bleached and fines-free sulphite birch pulp (Kappa number of 1, DP of 4700) suspended in distilled water at 1.8% (w/v). The suspension was disintegrated using a high-pressure fluidizer (Microfluidics M110P), the number of fluidizer passes is indicated with mechanically fibrillated CNFs (e.g. 9pCNF: 9 passes). Mechanically fibrillated CNFs are characterized by partial fibrillation, requiring care when interpreting simple dimensional characterizations (Mattos, Tardy, & Rojas, 2019). However, average dimensions of CNFs produced using the same materials and devices as in this work (with 6 fluidizer passes) have been determined: $1.46 \pm 0.8 \mu\text{m}$ length and $35 \pm 12 \text{ nm}$ diameter (Mattos et al., 2019). They typically have a slightly negative zeta potential from residual heteropolysaccharides bound to the surface, mainly xylans; a numerical value of -2 mV has been reported, for example (Lou et al., 2014; Toivonen et al., 2015). TEMPO-oxidized CNF (TOCNF) was prepared as described by Orelma et al. (2016). TOCNFs produced the same way as in this work have been characterized in earlier work, as having lengths of several microns and diameter equal to that of elementary fibrils of wood, i.e. $\sim 4 \text{ nm}$ (Beaumont et al., 2021). The charge content was 1.36 meq./g (Reyes et al., 2020). BSA and hen egg white lysozyme were purchased from Sigma-Aldrich. Sodium salt of CMC (MW 250 kDa, DS 1.2), and HPC (MW 100 kDa, DS 2.2 (Dubolazov, Nurkeeva, Mun, & Khutoryanskiy, 2006)) were purchased from Sigma-Aldrich. The following commercial adhesives were briefly tested for comparisons: Loctite Power Epoxy and Casco Express Gel, a cyanoacrylate adhesive.

2.1.1. Preparation of lap joints

Lap joints were chosen as the specimen to evaluate joint properties (Fig. 1). These were prepared by placing $20 \mu\text{L}$ of adhesive formulation onto a glass microscope slide (VWR International). The formulations were made by dissolving compounds into a volume of deionized water leading to the DMC aimed for. For combination formulations, the composition is indicated as the included components followed by the relative contents by weight for multiple components, e.g. CNF-CNC_{1:10}. Dry matter content (DMC, also called wt%) is also indicated when relevant, as a simple indicator of the formulation concentration, and complemented by the average areal density (mg/cm^2) of the produced joints. Another slide was then carefully placed on top of the liquid, to create a thin film between the two slides. The top slide was carefully levelled using a third glass slide to maintain planar contact. The overlap to be joined was ca. 25 mm wide and 10 mm long. The lap joints were then left to dry at room temperature, ca. 23% RH, for a minimum of 18 h before imaging and a minimum of 30 h before mechanical testing.

2.1.2. Imaging of joints

Joints were mostly photographed with a digital camera (10 MP resolution) in a dark room, illuminated with a fibre optic lamp (Fig. S1). The lysozyme and cellulose derivative-only joints were imaged on an Olympus SZX10 microscope without magnification.

Long range order was visualized using ordinary and polarized optical transmission microscopy (Olympus BX53M microscope), with the aid of a retardation plate (530 nm) to visualize relative orientation of the birefringent domains and increase the discernibility of details. The joints were imaged after drying, without further preparation steps.

Scanning electron microscopy (SEM) was used to image select representative samples, using a Zeiss Sigma VP device with a Schottky field emission source. The samples consisted of joints broken either under an in-plane or out-of-plane load (specified in the results), coated with a 4 nm thick layer of platinum/palladium alloy.

2.1.3. Adhesion tests of joints

Mechanical testing was performed with an MTS 400M tester. For in-plane adhesion measurements, samples were clamped with rough aluminium plates to provide enough grip without having to tighten the clamps excessively in order to protect the glass substrate and the brittle

joints. Although this strategy was also used to avoid slippage of the sample, it was not possible to completely eliminate such events given the high loads used and the submillimeter strain at break of the samples. Therefore, no toughness values are calculated in this work. The strain rate was set to 1.5 mm min^{-1} and the distance between clamps was kept at ca. 60 mm. The maximal load before failure was used to measure in-plane adhesion. It should be noted that among CNF-containing specimens, results would vary between tested sets, in a grouped manner. This may be due to particular susceptibility to changes in environment, such as humidity. Furthermore, consolidation required a considerably longer time ($>30 \text{ h}$ and typically 70 h) to obtain measurable strengths.

Out-of-plane adhesion was measured with the MTS 400M tester in compression mode (Fig. S2). The joint was clamped horizontally onto a thick aluminium plate with a bulldog clip and a thin piece of aluminium. A small steel plate was pushed down onto one glass slide near the joints border, to provide the out-of-plane load. This setup provides information on out-of-plane adhesion and toughness, with its geometry being reminiscent of the Boeing wedge test, which develops a crack in the material starting from one end. For HPC-only joints, the out-of-plane tests (OoPF) resulted in frequent substrate failure.

Surface coverage by the dried material within a joint was estimated using ImageJ analysis of joint photographs. The surface coverage values were employed for a more representative estimation of shear stress within the material, by assuming the surface coverage to be equivalent to the contact area between the adhesive material and the substrate. In other words, shear stress values were calculated in two different ways: (1) using the whole 2.5 cm^2 joint area ("lap shear stress"), and (2) using the estimated average surface coverage area for a given formulation ("ultimate shear stress"). The former corresponds with the common definition used in literature, while the latter gives more accurate insight into the adhesive material's properties.

We note that the dry matter content and areal densities within the overlap areas were maximized based on either substrate failure (maximum amount of bio-adhesive resulting in joint failure rather than substrate failure), gelation concentration (maximum concentration where the viscosity of the dispersion was sufficiently low to induce good wetting and therefore good adhesion), or chosen to facilitate comparison of formulations. For instance, BSA with CNCs at the same areal density as other samples ($0.44 \text{ mg}/\text{cm}^2$) led to in-plane adhesion that caused substrate failure in many of the specimens (non-substrate failure values averaged at 580 N). Due to this, BSA formulations were studied at a lower areal density of $0.2 \text{ mg}/\text{cm}^2$.

2.1.4. Gelation concentration estimation

The gelation behavior of the studied biomacromolecules was estimated through the vial inversion tests. A given amount of each compound was dissolved into 10 mL with deionized water in a ca. 2 cm wide glass vial, to concentrations of up to 50% (w/v). The gelation behavior was characterized by inverting the vial and observing whether the solution could flow downwards with only the force of gravity.

Additional details on experimental protocols described herein and deeper discussions on adhesive joints designs are accessible in the reference: Luotonen (2021).

3. Results and discussion

The various natural biopolymers studied herein showed very different behaviours under C-EISA, both when combined with CNCs and on their own (Fig. 2). Bio-macromolecules and bio-colloids can interact with themselves and other dissolved compounds as well as with the water-glass, and water-air interfaces where they will adsorb. The dynamics of the different interactions then affect joint formation, visible in such parameters as contact area within the overlap area and long-range order within microstructures. Upon placing a liquid formulation between two glass slides to form a joint, the solution is spread into a thin film in the slides' overlap. The initial thickness of the film has been

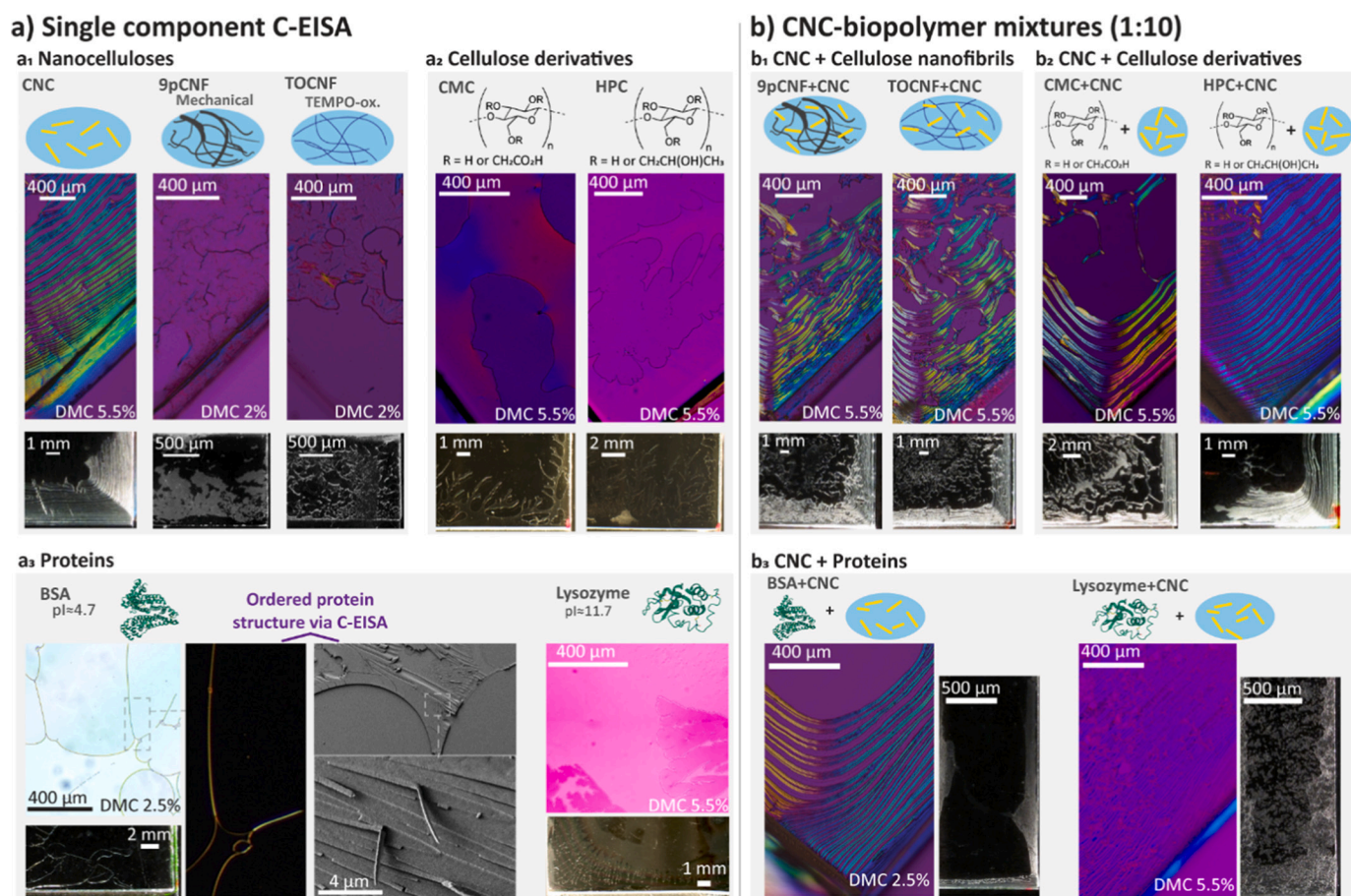


Fig. 2. Microscopy images (PLM images except for BSA-only joint) and photographs of studied joint. (a1) Joints from CNC (left) and CNFs (mechanical-left, TO-right). (a2) Joints containing CMC (left) and HPC (right). (a3) Joints from BSA as observed by optical microscopy (left) and SEM images (right). Lysozyme-based joints (far right, the brighter color is due to the stronger illumination required by the sample). (b1) Addition of CNFs to the CNC formulations (1:10). Microscopy images of 6pCNF and 12pCNF are included in SI (Fig. S4). (b2) Addition of CMC (left) and HPC (right) to CNC formulations (1:10). (b3) Addition of BSA (left) and lysozyme (right) to the CNC formulation.

estimated as ca. 80 μm , which then decreases during evaporation by factors of ca. 6 to 40 depending on DMC, assumed average density of the dried material, and relative coverage or contact area (Table S2).

As previously reported, CNCs produced well-ordered lamellae self-assembled at the joint rim (Fig. 2a1) (Tardy et al., 2020). The CNF-only joints showed smaller and less ordered birefringent domains within largely disordered assemblies (Fig. 2a1). These domains are larger and more apparent with TOCNF, compared to 9pCNF. CNFs were still capable of aligning on a local scale despite being arrested at the joint center earlier due to their lower gelation concentration (Table S1), which reduced the order formation within the joints. Compared to CNC-only joints, the addition of CNFs to CNCs (CNF:CNC_{1:10}) resulted in the additional formation of structures at the center of the joint, and the lamellae formation was disrupted (Fig. 2b1). Potentially as a result of the smaller fibril sizes, TOCNFs produced slightly better-resolved structures when combined with CNCs, with sharper patterns compared to the larger irregular spots seen with mechanically fibrillated CNFs.

On its own, BSA produced thin elongated strands and transparent films (Fig. 2a3). Such “fingering” patterns have been previously observed in similar systems (De Dier, Sempels, Hofkens, & Vermant, 2014; Reiter & Sharma, 2001; Vancea et al., 2008). BSA is known to be interfacially active and to maintain low viscosity even at high concentrations, which should benefit adhesion (Baldan, 2012; Suelter & DeLuca, 1983), as potentially associated with induced conformational changes (Glaeser & Han, 2017). Interestingly, the BSA strands showed birefringence, indicating the formation of long-range ordered multi-

domain crystals through C-EISA (Fig. S5). The overarching cause of these BSA-based strands is related to the work of adhesion of the dispersion, which is in balance with capillary flow in the concentrating dispersion (Greca et al., 2021). SEM images of BSA-only joints show an ordered inner structure of the protein, with a converging shape forming into a fine strand (Fig. 2a3). Droplets of BSA solution (2.5, 5, 10, 20% DMC) left to dry on an uncovered glass slide did not produce thin, birefringent strands as seen with C-EISA (Fig. S5), inferring that confinement is critical to develop localized crystallinity from protein constructs (Meldrum and O’Shaughnessy, 2020).

In contrast with BSA, lysozyme had a lower tendency to wet the substrate and foam when mixed, but by itself formed similar microstructures to BSA, with transparent films forming towards the joint center (Fig. 2b3). Thin “fingering” was also observed on the fringes. Unlike BSA, the lysozyme joints did not show clear birefringence and a number of small, polygonal-shaped aggregates could also be seen in lysozyme-only joints.

The combination of BSA with CNCs (10% relative DMC of BSA) had minimal impact on the formation of lamellae when compared to CNC alone (Fig. 2b3), although substructures were observed to delaminate within the lamellae (Fig. S6). Alternatively, the combination of lysozyme with CNCs (Lysozyme:CNC_{1:10}) heavily disrupted the formation of lamellae and caused larger surface coverage in the joint (Fig. 2b3). During the preparation of the formulations, small aggregates were seen in the mix of lysozyme and CNC (Fig. S3) that likely disrupted ordering during joint formation. This difference between BSA and lysozyme is

likely due to the isoelectric points of two, as lysozyme is positively charged at neutral pH (IP = 11.7 (Felsovalyi et al., 2011)). This positive charge leads to interactions with the negatively charged CNC surface (De France et al., 2020), as also shown with TOCNF (Wu et al., 2021), while the low viscosity of BSA (Roberts et al., 2020) (Table S1) and its negative charge (IP = 4.7 (Yasun et al., 2015)) minimize uncontrolled aggregation with CNCs. This suggests that controlling the charge of the additives and their potential to aggregate are prerequisites for assembling well-ordered structures (Bast et al., 2021).

CMC-only joints led to material being concentrated strongly along the joint edges showing long-range order (Fig. 2a2), despite CMC's higher viscosity compared to BSA or CNC (Table S1). Red or blue shades could be differentiated with CMC using a retardation plate, while similar behavior could not be observed with HPC. The differently coloured areas suggest local orientational differences in the material structure, corresponding with the orientation of the neighbouring drying fronts (Tardy et al., 2017). This behavior may be related to the more stretched conformation of CMC in solution, due to self-repulsion, compared to HPC. When used alone, despite the differences in long-range order and molecular conformation, HPC formed joints similar in macroscopic appearance to CMC (Fig. 2a2).

Interestingly, HPC-CNC mixtures (HPC:CNC_{1:10}) had low viscosity and resulted in largely undisturbed lamellae under C-EISA (Fig. 2b2). When CMC was combined with CNCs (CMC:CNC_{1:10}), lamellae could form relatively undisturbed, however a portion of the material was retained in the joint center (Fig. 2b2). The formulation partially aggregated with small-scale heterogeneity visible under the microscope (Fig. S3). The adsorption of CMC onto unmodified cellulose is well established (Butchosa & Zhou, 2014; Filpponen et al., 2012), and the gelation and flocculation of CNC dispersions by CMC has been reported and is thought to result from depletion forces in addition to supramolecular complexation (Oguzlu & Boluk, 2017; Su et al., 2020). The aggregates likely were large enough to arrest movement early in the drying process at the joint center in CMC:CNC_{1:10}, yet mobile and small enough to still produce long-range order and a birefringent structure under the stresses of the latter drying stages. Most importantly, the low degree of interactions of either of the components with glass prior to consolidation is likely to favor accumulation of the components towards the edges by capillary flow.

Correlation can be seen between joint morphology and gelation behaviour, when considering all tested bio-colloids and biomacromolecules. Specifically, the early-gelling CNFs cover the whole

joint area, while the intermediately gelling CNCs, CMC, and HPC migrate to the edges (Table S1). The protein, which gel at high concentrations, showed no preference towards accumulating at the joint edges as associated with their interfacial activity.

The adhesive performance of the different formulations was then evaluated both for in-plane and out-of-plane loads to determine whether the aforementioned structures influence adhesion. The ultimate in-plane force (lap-shear test) of each system are reported in Fig. 3 (see note in experimental section regarding DMC and areal concentration choices). The values of ultimate in-plane force (IPF) of CNC-only formulations corresponded with the contact area rather than DMC (albeit these are connected), as also previously reported (Tardy et al., 2020).

The addition of CNFs to CNCs (CNF:CNC_{1:10}) produced no measurable improvement. For mechanically fibrillated CNFs, average in-plane adhesion increased with the number of fluidizer passes (215 N, 261 N, 323 N for 6, 9 and 12 passes, respectively), corresponding to increased adhesion with higher degrees of fibrillation. Interestingly, the out-of-plane adhesion values were consistent across the different fibrillation degrees (17 N, 12 N, 13 N on average), suggesting that lower fibrillation degree, and thus size, result in proportionally higher toughness. This may suggest higher entanglement for partially fibrillated systems. In comparison with the mechanically fibrillated CNFs, TOCNF (which has the highest degree of fibrillation) showed lower adhesion both in-plane and out-of-plane (21 N and 3.7 N on average, respectively). This surprising result could potentially be ascribed to the heteropolysaccharide content of the mechanical CNFs, which may provide additional fibril-fibril and fibril-substrate hydrogen bonding, given their native role as lignin-cellulose linkers (Terashima et al., 2009). Another factor at play may be the high areal charge density of TOCNF hindering cohesion and adhesion. The less stabilized mechanical CNFs may also be more prone to consolidation, particularly under capillary stresses.

The adhesion of BSA on its own corresponded with previously reported values (on the order of 10 MPa) (Roberts et al., 2020), where it was hypothesized that changes in conformation were important for the development of adhesive strength. In their work, Roberts et al. found that upon dehydration BSA transitions from an α -helix rich to a β -sheet rich (72.1% to 6.7% helical, 24.8% to 48.5% sheet) state, proposing the formation of quaternary β -sheet structures. In supramolecular assembly β -sheet structures are generally capable of interacting via van der Waals, hydrophobic, or hydrogen bonds (Cheng, Pham, & Nowick, 2013). The former two are however associated with good shape complementarity, and the glass substrate's surface may also lend itself more to hydrogen

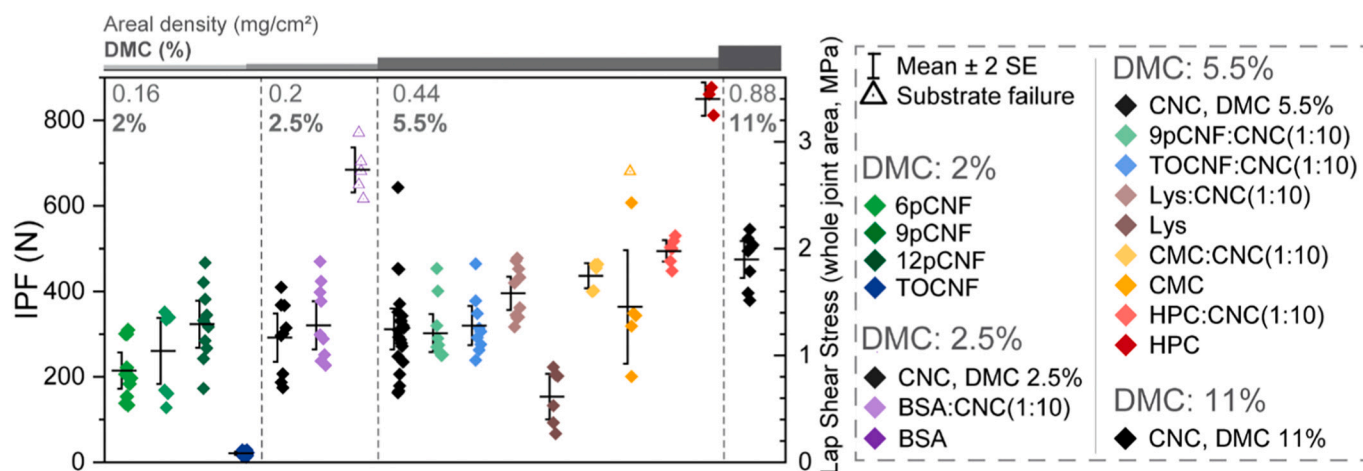


Fig. 3. Ultimate in-plane force (IPF) of joints, corresponding with in-plane adhesion (SE: standard error). Overall lap shear area strength values are indicated on the secondary axis, and were calculated based on the surface area of the whole joint. Areal density values and the corresponding DMC are also included. Values associated with substrate failure are included when representing the highest obtained value or more than half of the recorded values, meaning the average underestimate the true strength of the concerned joint when substrate failure occurs. Additional benchmarks of biopolymeric adhesives including starch and gelatine can be accessed in a previous study (Greca et al., 2021).

bonding. On the other hand, lysozyme on its own consistently showed low adhesion (154 ± 65 N), potentially due to its higher chemical stability hindering formation of a good adhesive joint where its conformation is less affected by adsorption (Sethuraman, Vedantham, Imoto, Przybycien, & Belfort, 2004), as the protein has evolved to withstand relatively harsh extracellular conditions (Felsevalyi et al., 2011). The poor adhesive performance of lysozyme and TOCNF, both relatively charged species, may suggest hindrance of joint formation by their coulombic repulsion. While lysozyme has also been found to transition to a more β -sheet rich conformation upon adsorption, this happens clearly to a lesser extent (-20% helical content, $+10\%$ sheet content) (Felsevalyi et al., 2011). The change in conformation is also reportedly reversible upon desorption, as opposed to BSA which may not fully recover (Norde & Favier, 1992). However, lysozyme could still be used as an additive to CNCs that resulted in a 27% improvement (lysozyme: CNC_{1:10}) to in-plane adhesion when compared to pristine CNCs.

On their own, CMC and HPC showed average in-plane adhesion values of 364 N and 850 N, respectively. However, the CMC formulation showed high variability with a standard deviation of 149 N, possibly due to its higher viscosity hindering consistent and uniform joint coverage. Still, the addition of CMC to CNCs (CMC:CNC_{1:10}) produced a synergistic improvement (40%) on the mean, as the combined formulation showed much less variance in strength. Similarly, HPC improved the adhesion by 59% when compared with CNC-only joints, likely due to its ability to intercalate into and reinforce the CNC structure. This result was supported by previous findings where composite films formed with CNCs could be strengthened by HPC (Walters et al., 2020). HPC is amphiphilic with a high wettability and foam stabilization due to its air-water interactions, which may be partly responsible for the better performance compared to CMC. Both cellulose derivatives have the capability to form supramolecular hydrogen bonds in principle via their side groups, but the higher degree of substitution of the employed HPC grade may provide more OH-groups spaced away from the immediate vicinity, and the sodium ions of the employed CMC grade could possibly further lower the possibility of hydrogen-bonding.

Commercial adhesives (Loctite Power Epoxy; Casco Express Gel, a cyanoacrylate adhesive) were tested under in-plane loads for comparison with the studied formulations. Roughly equivalent amounts were used in terms of dry matter remaining in the joint, albeit the high DMC

and viscosity of the adhesives made accurate use difficult and likely caused some overshoot in areal density. The cyanoacrylate adhesive generally failed at loads of 600 N and beyond, while the epoxy-based joints failed at similar loads when failing at the joint, but experienced substrate failure in about half of the joints. Some of the bio-based formulations performed remarkably well compared to the commercial products' in-plane adhesion, which is noteworthy as the adhesion mechanisms of the bio-based formulations are strictly non-covalent interactions. Although the optimized commercial formulations would be expected to have better in-plane performance than the simple formulations studied herein, our results demonstrate the significant promise of bio-adhesives where the potential for cumulatively strong non-covalent interactions is successfully harnessed. When compared with high-performance synthetic adhesives, the water resistance of natural polymer-based materials generally require caution. For example, cellulose materials which can present e.g. tensile strengths on the order of 1 GPa and beyond (Mittal et al., 2017; Mittal et al., 2018) drastically lose cohesion when wet if unprotected against water effects (Bensselfelt, Engström, & Wågberg, 2018; Lundahl et al., 2016). Efforts have been put forward to address this (Bensselfelt et al., 2018; Lundahl et al., 2016), but significant challenges remain if significant up-scaling is to be achieved.

The anisotropies of most joints were quite consistent at 10–20-fold, i. e. the ultimate out-of-plane loads shown by different formulations appear to be correlated with the in-plane loads (Fig. 4b). Interestingly, our results with CNC-only joints deviate from our earlier work (Tardy et al., 2020) in that the in-plane adhesion values were comparable (ca. -20% herein), however the out-of-plane load was substantially different, resulting in an anisotropy with lower upper boundaries. This is likely associated with the specific cellulose used in this study having different physicochemical properties (e.g. presence of cellulose II to varying amount and possible dimension differences), which suggests that significant further work is required to truly understand the formation, adhesion, and cohesion mechanisms of CNC (Reid et al., 2017). BSA-only joints (not shown in Fig. 4) presented an outlier compared to other tested compounds, with a lower bound of ca. 50-fold anisotropy.

TOCNF may be an interesting additive to improve out-of-plane adhesion if the variability can be mitigated based on the upper outliers obtained with TOCNF and CNC joints (with values of ca. 30–40 N in TOCNF:CNC_{1:10} joints) (Mattos et al., 2020). While the HPC:CNC_{1:10}

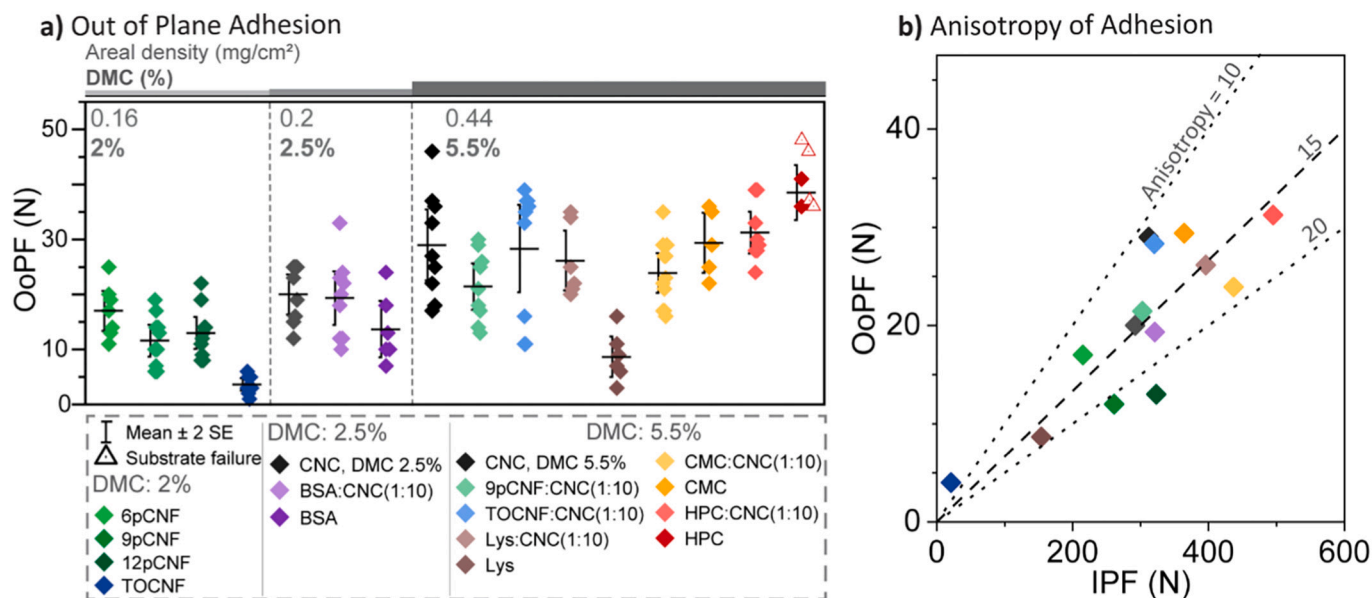


Fig. 4. (a) Ultimate out-of-plane force (OoPF) of joints, representing out-of-plane adhesion. Areal density and corresponding DMC values are included. Values associated with substrate failure are included when representing the highest obtained value or more than half of recorded values. These underestimate the true strength of the concerned joint. (b) Comparison of OoPF and IPF for different formulations, with visualized corresponding anisotropy values. BSA and HPC-only joints are not included, due to the high number of corresponding substrate failures.

formulation did not change the out-of-plane adhesion strength much compared to CNC-only joints, using only HPC produced consistently higher ultimate load values of 40–50 N (possibly due to the gradual failure observed with HPC-only joints in the in-plane adhesion tests (IPF measurement)). Specifically, the gradual undoing of the patterns in the joint could be readily observed, lasting from a few to over ten seconds. This contrasts with the other systems, which would emit audible fractures before failure, suggesting more brittle joints overall. The delayed failure mode of HPC-only joints relieves strain and increase the overall toughness of the joint. The delayed fracture also allowed for a higher load to be reached under out-of-plane loading (with most failures finally occurring in the substrate), which translates into a lower anisotropy of adhesion. In most of these high strength joints the substrate was first to fail, in which case only a minimum value could be defined for the compound's performance, suggesting that HPC is a promising additive along with TOCNF.

In addition to further studies regarding the bio-colloids and biomacromolecules as described herein, the effects of modifying substrate surface chemistry and the impact of inorganic fillers comprise potential future work of interest. The related formation of superstructured particles between CNFs and various inorganic or organic fillers have been studied in earlier work (Mattos et al., 2020).

For more in-depth characterization of the studied formulations, ultimate shear stress values were also estimated based on the in-plane force and the actual surface coverage within the joint (Fig. 5) as estimated using image processing software (Fig. S7). As the maximal IPF values reflect the optimal adhesion performance more closely, stress values were calculated based both on average and maximal IPF for each formulation. In particular, BSA and HPC showed high ultimate shear stress when estimated this way (beyond 10 MPa); note that the values are underestimated for BSA-only joints due to the IPF values corresponding to the substrate failure and not the joint failure as the latter rarely occurred before substrate failure. The two biomacromolecules were followed in performance by CNC, and CMC, and finally by CNFs and lysozyme. Interestingly, the ultimate shear stress values for pure CNC deviated from our previous work, where the 5.5% DMC formulation (equal to 0.44 mg/cm² loading) was slightly higher our previous study (Tardy et al., 2020), while the 11% DMC formulation (equal to 0.88 mg/cm² loading) produced significantly lower values, further suggesting a significant impact from the physico-chemical properties of CNFs that still needs to be elucidated.

The addition of 10% of HPC resulted in the most significant improvement of CNC adhesives (strength improved by 72%). Addition of CMC to CNFs left the joint strength mostly unchanged. In comparison, other compounds resulted in a decreased of shear strength when

normalized to the contact area. The low shear stresses seen for CNF: CNC_{1:10} and Lysozyme:CNC_{1:10} formulations (2 and 2.6 MPa for 9pCNF and TOCNF resp., 2.6 MPa for lysozyme) corresponded with their higher surface coverage and proportionally lower loads at failure. In addition to error stemming from the limits of resolving the fine structures in some joints, not all dried material necessarily makes contact between both substrates and participates in load transfer, suggesting our calculated values could be underestimations.

Overall the remarkable performance of BSA suggests specific transitions into higher order secondary, tertiary, or quaternary structures during consolidation of the biopolymers. Regarding bio-colloids, the disappearance of continuous microstructures (i.e. lamellae) and decrease of large-scaled alignment systematically resulted in lower adhesion strengths. However, in the case of dissolved biopolymers such correlation did not occur, suggesting that intimate contact with the substrate was promoted by alignment in the case bio-colloids and resulted in higher adhesive strengths while for biopolymers the functional groups and gelation behavior of the polymer were more critical than their overall relative long-range order.

4. Conclusion

In this study we have evaluated three specific types of biopolymers including nanocelluloses (bio-colloids), proteins, and cellulose derivatives for their adhesion performance as single components or when used as an additive to CNFs. Interestingly, the performance varied significantly among biopolymers without clear structure-functionality relationship. Higher gelling concentrations, and the resulting formation of long-range order in the joint were generally associated with higher in-plane adhesion strength. When examining the glass-biopolymer interface for single compounds, BSA and HPC showed excellent adhesion, above 10 MPa, with the next best performers being CMC, and CNFs at ca. 5 MPa, and lysozyme and TOCNF showing relatively poor performances. CNFs performed relatively well on their own (ca. 2 MPa), with increased performance at higher fibrillation. Composite joints of CNFs with 10% of additive showed varied results, with HPC improving performance the most overall (ultimate shear stress by 72%, out-of-plane load by 33%), and TOCNFs showing potential promise in improving out-of-plane adhesion. Other important considerations should be put forward when choosing optimal building blocks for adhesions such as sourcing (by-products vs high value macromolecules), cost-competitiveness, and scale of production. The latter two are correlated, which underpins the current low competitiveness of nanocelluloses due to their current high prices and lower performance when comparing, for instance, with HPC. When comparing the anisotropy of adhesion, a consistent 10–20-fold anisotropy was observed across most systems that scaled linearly with the strength of the joint, suggesting that the anisotropy of these bio-adhesives relates fundamentally to their non-covalent nature rather than the specific physicochemical properties of the build blocks. This is consistent with the isotropy of adhesion of covalent adhesives. Importantly, this work presents the only current benchmark for the range of materials evaluated herein, where their interactions at interfaces can be readily compared alone and as composites. As this field progresses, a more comprehensive property space of the interfacial adhesive strength of natural biopolymers will provide guidelines for the formation of composites as well as for the formation of green adhesives, optimizing costs, sustainability, and performance.

CRedit authorship contribution statement

Otso I.V. Luotonen: Formal analysis, Investigation, Writing – original draft, Writing – review & editing. **Luiz G. Greca:** Supervision, Formal analysis, Investigation, Writing – original draft, Conceptualization. **Gustav Nyström:** Investigation, Writing – review & editing. **Junling Guo:** Writing – review & editing, Conceptualization. **Joseph J. Richardson:** Writing – review & editing, Conceptualization. **Orlando J.**

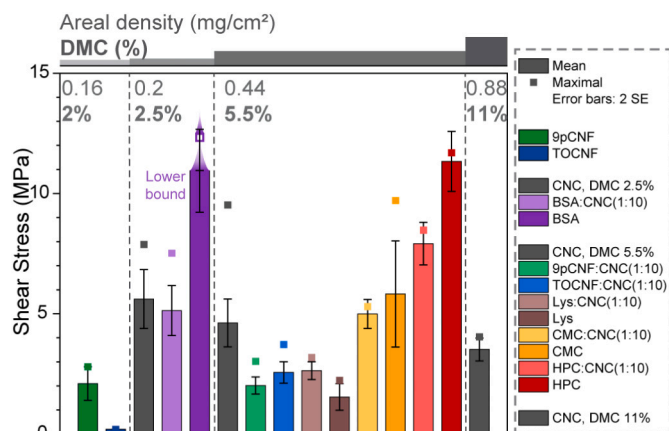


Fig. 5. Estimated ultimate shear stress values. Values were calculated based both on average and maximal IPF values, and the estimated contact area (lower bounds are described for BSA).

Rojas: Supervision, Resources, Writing – review & editing, Funding acquisition. **Blaise L. Tardy:** Supervision, Conceptualization, Writing – original draft, Writing – review & editing, Methodology.

Declaration of competing interest

The authors declare that they have no known competing financial interests or personal relationships that could have appeared to influence the work reported in this paper.

Acknowledgements

The authors acknowledge the provision of facilities and technical support by Aalto University at OtaNano - Nanomicroscopy Center (Aalto-NMC), as well as Aalto Takeout for lending camera equipment. This work received funding from the European Research Council (ERC) under the European Union's Horizon 2020 research and innovation programme (grant agreement No 788489, "BioElCell"). GN also acknowledges funding from the Swiss National Science Foundation (Grant No. 200021_192225). JJR acknowledges JSPS for the postdoctoral fellowship for research in Japan (P20373).

Appendix A. Supplementary data

Supplementary data to this article can be found online at <https://doi.org/10.1016/j.carbpol.2022.119681>.

References

- Ajdary, R., Tardy, B. L., Mattos, B. D., Bai, L., & Rojas, O. J. (2021). Plant nanomaterials and inspiration from nature: Water interactions and hierarchically structured hydrogels. *Advanced Materials*, 33(28), 2001085. <https://doi.org/10.1002/adma.202001085>
- Baldan, A. (2012). Adhesion phenomena in bonded joints. *International Journal of Adhesion and Adhesives*, 38, 95–116. <https://doi.org/10.1016/j.ijadhadh.2012.04.007>
- Bast, L. K., Klockars, K. W., Greca, L. G., Rojas, O. J., Tardy, B. L., & Bruns, N. (2021). Infiltration of proteins in cholesteric cellulose structures. *Biomacromolecules*, 22(5), 2067–2080. <https://doi.org/10.1021/acs.biomac.1c00183>
- Beaumont, M., Tardy, B. L., Reyes, G., Koso, T. V., Schaubmayr, E., Jusner, P., King, A. W. T., Dagastine, R. R., Potthast, A., Rojas, O. J., & Rosenau, T. (2021). Assembling native elementary cellulose nanofibrils via a reversible and regioselective surface functionalization. *Journal of the American Chemical Society*, 143(41), 17040–17046. <https://doi.org/10.1021/jacs.1c06502>
- Beisl, S., Adamczyk, J., Friedl, A., & Ejima, H. (2020). Confined evaporation-induced self-assembly of colloidal lignin particles for anisotropic adhesion. *Colloid and Interface Science Communications*, 38, Article 100306. <https://doi.org/10.1016/j.colcom.2020.100306>
- Benselfelt, T., Engström, J., & Wågberg, L. (2018). Supramolecular double networks of cellulose nanofibrils and algal polysaccharides with excellent wet mechanical properties. *Green Chemistry*, 20(11), 2558–2570. <https://doi.org/10.1039/C8GC00590G>
- Butchosa, N., & Zhou, Q. (2014). Water redispersible cellulose nanofibrils adsorbed with carboxymethyl cellulose. *Cellulose*, 21(6), 4349–4358. <https://doi.org/10.1007/s10570-014-0452-7>
- Chen, F., Xiang, W., Sawada, D., Bai, L., Hummel, M., Sixta, H., & Budtova, T. (2020). Exploring large ductility in cellulose nanopaper combining high toughness and strength. *ACS Nano*, 14(9), 11150–11159. <https://doi.org/10.1021/acsnano.0c02302>
- Cheng, H. N., Wyckoff, W., Dowd, M. K., & He, Z. (2019). Evaluation of adhesion properties of blends of cottonseed protein and anionic water-soluble polymers. *Journal of Adhesion Science and Technology*, 33(1), 66–78. <https://doi.org/10.1080/01694243.2018.1495404>
- Cheng, P.-N., Pham, J. D., & Nowick, J. S. (2013). The supramolecular chemistry of β -sheets. *Journal of the American Chemical Society*, 135(15), 5477–5492. <https://doi.org/10.1021/ja3088407>
- Cole, M., Lindeque, P., Halsband, C., & Galloway, T. S. (2011). Microplastics as contaminants in the marine environment: A review. *Marine Pollution Bulletin*, 62(12), 2588–2597. <https://doi.org/10.1016/j.marpolbul.2011.09.025>
- Daicho, K., Kobayashi, K., Fujisawa, S., & Saito, T. (2021). Recovery of the irreversible crystallinity of nanocellulose by crystallite fusion: A strategy for achieving efficient energy transfers in sustainable biopolymer Skeletons**. *Angewandte Chemie International Edition*, 60(46), 24630–24636. <https://doi.org/10.1002/anie.202110032>
- De Dier, R., Sempels, W., Hofkens, J., & Vermant, J. (2014). Thermocapillary fingering in surfactant-laden water droplets. *Langmuir*, 30(44), 13338–13344. <https://doi.org/10.1021/la503655j>
- De France, K. J., Kummer, N., Ren, Q., Campioni, S., & Nyström, G. (2020). Assembly of cellulose nanocrystal-lysozyme composite films with varied lysozyme morphology. *Biomacromolecules*, 21(12), 5139–5147. <https://doi.org/10.1021/acs.biomac.0c01267>
- Dore, C., Dörfling, B., Garcia-Pomar, J. L., Campoy-Quiles, M., & Mihi, A. (2020). Hydroxypropyl cellulose adhesives for transfer printing of carbon nanotubes and metallic nanostructures. *Small*, 16(47), 2004795. <https://doi.org/10.1002/sml.202004795>
- Dubolazov, A. V., Nurkeeva, Z. S., Mun, G. A., & Khutoryanskiy, V. V. (2006). Design of Mucoadhesive Polymeric Films Based on blends of Poly(acrylic acid) and (Hydroxypropyl)cellulose. *Biomacromolecules*, 7(5), 1637–1643. <https://doi.org/10.1021/bm060090l>
- Espinha, A., Dore, C., Matricardi, C., Alonso, M. I., Goñi, A. R., & Mihi, A. (2018). Hydroxypropyl cellulose photonic architectures by soft nanoimprinting lithography. *Nature Photonics*, 12(6), 343–348. <https://doi.org/10.1038/s41566-018-0152-1>
- Felsovalyi, F., Mangiagalli, P., Bureau, C., Kumar, S. K., & Banta, S. (2011). Reversibility of the adsorption of lysozyme on silica. *Langmuir*, 27(19), 11873–11882. <https://doi.org/10.1021/la202585r>
- Filpponen, I., Kontturi, E., Nummelin, S., Rosilo, H., Kolehmainen, E., Ikkala, O., & Laine, J. (2012). Generic method for modular surface modification of cellulosic materials in aqueous medium by sequential "Click" reaction and adsorption. *Biomacromolecules*, 13(3), 736–742. <https://doi.org/10.1021/bm201661k>
- Gençer, A., Schütz, C., & Thielemans, W. (2017). Influence of the particle concentration and marangoni flow on the formation of cellulose nanocrystal films. *Langmuir*, 33(1), 228–234. <https://doi.org/10.1021/acs.langmuir.6b03724>
- Geyer, R., Jambbeck, J. R., & Law, K. L. (2017). Production, use, and fate of all plastics ever made. *Science Advances*, 3(7), Article e1700782. <https://doi.org/10.1126/sciadv.1700782>
- Greca, G. L., France, K. J. D., Majoinen, J., Kummer, N., Luotonen, V., OI, Campioni, S., Rojas, J. O., Nyström, O. G., & Tardy, L. B. (2021). Chitin–amyloid synergism and their use as sustainable structural adhesives. *Journal of Materials Chemistry A*. <https://doi.org/10.1039/D1TA03215A>
- Glaeser, R. M., & Han, B.-G. (2017). Opinion: Hazards faced by macromolecules when confined to thin aqueous films. *Biophysics Reports*, 3(1), 1–7. <https://doi.org/10.1007/s41048-016-0026-3>
- Klockars, K. W., Yau, N. E., Tardy, B. L., Majoinen, J., Kämäräinen, T., Miettunen, K., Boutonnet, E., Borghei, M., Beidler, J., & Rojas, O. J. (2019). Asymmetrical coffee rings from cellulose nanocrystals and prospects in art and design. *Cellulose*, 26(1), 491–506. <https://doi.org/10.1007/s10570-018-2167-7>
- Korhonen, O., Sawada, D., & Budtova, T. (2019). All-cellulose composites via short-fiber dispersion approach using NaOH–water solvent. *Cellulose*, 26(8), 4881–4893. <https://doi.org/10.1007/s10570-019-02422-z>
- Li, T., Chen, C., Brozana, A. H., Zhu, J. Y., Xu, L., Driemeier, C., Dai, J., Rojas, O. J., Isogai, A., Wågberg, L., & Hu, L. (2021). Developing fibrillated cellulose as a sustainable technological material. *Nature*, 590(7844), 47–56. <https://doi.org/10.1038/s41586-020-03167-7>
- Lou, Y.-R., Kanninen, L., Kuisma, T., Niklander, J., Noon, L. A., Burks, D., Urtti, A., & Yliperttula, M. (2014). The use of nanofibrillar cellulose hydrogel as a flexible three-dimensional model to culture human pluripotent stem cells. *Stem Cells and Development*, 23(4), 380–392. <https://doi.org/10.1089/scd.2013.0314>
- Lundahl, M. J., Cunha, A. G., Rojo, E., Papageorgiou, A. C., Rautkari, L., Arboleda, J. C., & Rojas, O. J. (2016). Strength and water interactions of cellulose I filaments wet-spun from cellulose nanofibril hydrogels. *Scientific Reports*, 6(1), 30695. <https://doi.org/10.1038/srep30695>
- Luotonen, O. *Performance of bio-colloids as structural adhesives: Effect of nanoscaled morphology and polymeric additives* [Aalto University]. <http://urn.fi/URN:NBN:fi:aalto-202110249700>
- Mattos, B. D., Tardy, B. L., Greca, L. G., Kämäräinen, T., Xiang, W., Cusola, O., Magalhães, W. L. E., & Rojas, O. J. (2020). Nanofibrillar networks enable universal assembly of superstructured particle constructs. *Science Advances*, 6(19), Article eaaz7328. <https://doi.org/10.1126/sciadv.aaz7328>
- Mattos, B. D., Tardy, B. L., & Rojas, O. J. (2019). Accounting for substrate interactions in the measurement of the dimensions of cellulose nanofibrils. *Biomacromolecules*, 20(7), 2657–2665. <https://doi.org/10.1021/acs.biomac.9b00432>
- Meldrum, F. C., & O'Shaughnessy, C. (2020). Crystallization in confinement. *Advanced Materials*, 32(31), 2001068. <https://doi.org/10.1002/adma.202001068>
- Mittal, K. L., & Pizzi, A. (2003). Testing of adhesives. In *Handbook of Adhesives Technology* (2nd ed.). CRC Press LLC <http://ebookcentral.proquest.com/lib/aalto-ebooks/detail.action?docID=215918>
- Mittal, N., Ansari, F., Gowda, V. K., Brouzet, C., Chen, P., Larsson, P. T., Roth, S. V., Lundell, F., Wågberg, L., Kotov, N. A., & Söderberg, L. D. (2018). Multiscale control of nanocellulose assembly: Transferring remarkable nanoscale fibril mechanics to macroscale fibers. *ACS Nano*, 12(7), 6378–6388. <https://doi.org/10.1021/acsnano.8b01084>
- Mittal, N., Jansson, R., Widhe, M., Benselfelt, T., Håkansson, K. M. O., Lundell, F., Hedhammar, M., & Söderberg, L. D. (2017). Ultrastrong and bioactive nanostructured bio-based composites. *ACS Nano*, 11(5), 5148–5159. <https://doi.org/10.1021/acsnano.7b02305>
- Natarajan, B., Krishnamurthy, A., Qin, X., Emiroglu, C. D., Forster, A., Foster, E. J., Weder, C., Fox, D. M., Keten, S., Obrzut, J., & Gilman, J. W. (2018). Binary cellulose nanocrystal blends for bioinspired damage tolerant photonic films. *Advanced Functional Materials*, 28(26), 1800032. <https://doi.org/10.1002/adfm.201800032>
- Norde, W., & Favier, J. P. (1992). Structure of adsorbed and desorbed proteins. *Colloids and Surfaces*, 64(1), 87–93. [https://doi.org/10.1016/0166-6622\(92\)80164-W](https://doi.org/10.1016/0166-6622(92)80164-W)

- Oguzlu, H., & Boluk, Y. (2017). Interactions between cellulose nanocrystals and anionic and neutral polymers in aqueous solutions. *Cellulose*, 24(1), 131–146. <https://doi.org/10.1007/s10570-016-1096-6>
- Orelma, H., Vuoriluoto, M., Johansson, L.-S., Campbell, J. M., Filpponen, I., Biesalski, M., & Rojas, O. J. (2016). Preparation of photoreactive nanocellulosic materials via benzophenone grafting. *RSC Advances*, 6(88), 85100–85106. <https://doi.org/10.1039/C6RA15015B>
- Reid, M. S., Villalobos, M., & Cranston, E. D. (2017). Benchmarking cellulose nanocrystals: From the laboratory to industrial production. *Langmuir*, 33(7), 1583–1598. <https://doi.org/10.1021/acs.langmuir.6b03765>
- Reiter, G., & Sharma, A. (2001). Auto-optimization of dewetting rates by rim instabilities in slipping polymer films. *Physical Review Letters*, 87(16), Article 166103. <https://doi.org/10.1103/PhysRevLett.87.166103>
- Reyes, G., Lundahl, M. J., Alejandro-Martín, S., Artega-Pérez, L. E., Oviedo, C., King, A. W. T., & Rojas, O. J. (2020). Coaxial spinning of all-cellulose Systems for Enhanced Toughness: Filaments of oxidized nanofibrils sheathed in cellulose II regenerated from a protic ionic liquid. *Biomacromolecules*, 21(2), 878–891. <https://doi.org/10.1021/acs.biomac.9b01559>
- Roberts, A. D., Finnigan, W., Kelly, P. P., Faulkner, M., Breitling, R., Takano, E., Scrutton, N. S., Blaker, J. J., & Hay, S. (2020). Non-covalent protein-based adhesives for transparent substrates—bovine serum albumin vs. recombinant spider silk. *Materials Today Bio*, 7, 100068. <https://doi.org/10.1016/j.mtbio.2020.100068>
- Sethuraman, A., Vedantham, G., Imoto, T., Przybycien, T., & Belfort, G. (2004). Protein unfolding at interfaces: Slow dynamics of α -helix to β -sheet transition. *Proteins: Structure, Function, and Bioinformatics*, 56(4), 669–678. <https://doi.org/10.1002/prot.20183>
- Siqueira, G., Kokkinis, D., Libanori, R., Hausmann, M. K., Gladman, A. S., Neels, A., Tingaut, P., Zimmermann, T., Lewis, J. A., & Studart, A. R. (2017). Cellulose nanocrystal inks for 3D printing of textured cellular architectures. *Advanced Functional Materials*, 27(12), 1604619. <https://doi.org/10.1002/adfm.201604619>
- Su, F., Liu, D., Li, M., Li, Q., Liu, C., Liu, L., He, J., & Qiao, H. (2020). Mesophase transition of cellulose nanocrystals aroused by the incorporation of two cellulose derivatives. *Carbohydrate Polymers*, 233, Article 115843. <https://doi.org/10.1016/j.carbpol.2020.115843>
- Suelter, C. H., & DeLuca, M. (1983). How to prevent losses of protein by adsorption to glass and plastic. *Analytical Biochemistry*, 135(1), 112–119. [https://doi.org/10.1016/0003-2697\(83\)90738-8](https://doi.org/10.1016/0003-2697(83)90738-8)
- Tardy, B. L., Ago, M., Guo, J., Borghei, M., Kämäräinen, T., & Rojas, O. J. (2017). Optical properties of self-assembled cellulose nanocrystals films suspended at planar-symmetrical interfaces. *Small*, 13(47), 1702084. <https://doi.org/10.1002/sml.201702084>
- Tardy, B. L., Mattos, B. D., Otoni, C. G., Beaumont, M., Majoinen, J., Kämäräinen, T., & Rojas, O. J. (2021). Deconstruction and reassembly of renewable polymers and biocolloids into next generation structured materials. *Chemical Reviews*. <https://doi.org/10.1021/acs.chemrev.0c01333>
- Tardy, B. L., Richardson, J. J., Greca, L. G., Guo, J., Ejima, H., & Rojas, O. J. (2020). Exploiting supramolecular interactions from polymeric colloids for strong anisotropic adhesion between solid surfaces. *Advanced Materials*, 32(14), 1906886. <https://doi.org/10.1002/adma.201906886>
- Terashima, N., Kitano, K., Kojima, M., Yoshida, M., Yamamoto, H., & Westermark, U. (2009). Nanostructural assembly of cellulose, hemicellulose, and lignin in the middle layer of secondary wall of ginkgo tracheid. *Journal of Wood Science*, 55(6), 409–416. <https://doi.org/10.1007/s10086-009-1049-x>
- Toivonen, M. S., Kurki-Suonio, S., Schacher, F. H., Hietala, S., Rojas, O. J., & Ikkala, O. (2015). Water-resistant, transparent hybrid nanopaper by physical cross-linking with chitosan. *Biomacromolecules*, 16(3), 1062–1071. <https://doi.org/10.1021/acs.biomac.5b00145>
- Vancea, I., Thiele, U., Pauliac-Vaujour, E., Stannard, A., Martin, C. P., Blunt, M. O., & Moriarty, P. J. (2008). Front instabilities in evaporatively dewetting nanofluids. *Physical Review E*, 78(4), Article 041601. <https://doi.org/10.1103/PhysRevE.78.041601>
- Walters, C. M., Boott, C. E., Nguyen, T.-D., Hamad, W. Y., & MacLachlan, M. J. (2020). Iridescent cellulose nanocrystal films modified with hydroxypropyl cellulose. *Biomacromolecules*, 21(3), 1295–1302. <https://doi.org/10.1021/acs.biomac.0c00056>
- Wang, Y., Jia, K., Xiang, C., Yang, J., Yao, X., & Suo, Z. (2019). Instant, tough, noncovalent adhesion. *ACS Applied Materials & Interfaces*, 11(43), 40749–40757. <https://doi.org/10.1021/acsami.9b10995>
- Wu, T., Kummer, N., De France, K. J., Campioni, S., Zeng, Z., Siqueira, G., Dong, J., & Nyström, G. (2021). Nanocellulose-lysozyme colloidal gels via electrostatic complexation. *Carbohydrate Polymers*, 251, Article 117021. <https://doi.org/10.1016/j.carbpol.2020.117021>
- Yang, X., Biswas, S. K., Han, J., Tanpichai, S., Li, M.-C., Chen, C., Zhu, S., Das, A. K., & Yano, H. (2021). Surface and Interface engineering for nanocellulosic advanced materials. *Advanced Materials*, 33(28), 2002264. <https://doi.org/10.1002/adma.202002264>
- Yasun, E., Li, C., Barut, I., Janvier, D., Qiu, L., Cui, C., & Tan, W. (2015). BSA modification to reduce CTAB induced nonspecificity and cytotoxicity of aptamer-conjugated gold nanorods. *Nanoscale*, 7(22), 10240–10248. <https://doi.org/10.1039/C5NR01704A>
- Yi, H., Lee, S.-H., Ko, H., Lee, D., Bae, W.-G., Kim, T., Hwang, D. S., & Jeong, H. E. (2019). Ultra-adaptable and wearable photonic skin based on a shape-memory, responsive cellulose derivative. *Advanced Functional Materials*, 29(34), 1902720. <https://doi.org/10.1002/adfm.201902720>